ELSEVIER

Journal of Biomechanics 39 (2006) 1842–1851

JOURNAL OF BIOMECHANICS

www.elsevier.com/locate/jbiomech
www.JBiomech.com

Collagen fiber orientation at the tendon to bone insertion and its influence on stress concentrations

Stavros Thomopoulos[a,*], Juan P. Marquez[a], Bradley Weinberger[a], Victor Birman[b], Guy M. Genin[a]

[a]*Department of Orthopaedic Surgery, Washington University, 1 Barnes-Jewish Hospital Plaza, Suite 11300, Campus Box 8233, St. Louis, MO 63110, USA*

[b]*University of Missouri—Rolla, Engineering Education Center, St. Louis, MO 63121, USA*

Accepted 20 May 2005

Abstract

The tendon to bone insertion serves the mechanical role of transferring loads from a relatively compliant tendon to a relatively rigid bone. The details of the mechanism of load transfer are of great importance, since current surgical procedures for tendon reattachment have high failure rates. We hypothesized that the microscopic structure of the insertion is optimized to minimize stress concentrations associated with this load transfer. To explore this, collagen fiber orientation distributions were measured in the supraspinatus tendons of rats. The angular deviation of fibers was fairly uniform across the insertion, and the mean angles of the local distributions deviated mildly from the tendon axis. To explore how these observed property distributions could influence load transfer, these distributions were used to derive material properties for an idealized two-dimensional mechanical model of an insertion. Comparison between stress concentrations in this idealized model and those in three comparison models suggests that the microstructure serves to (1) simultaneously reduce stress concentrations and material mass, and (2) shield the insertion's outward splay from the highest stresses.

Keywords: Tendon; Insertion site; Stress concentration; Modeling; Collagen

1. Introduction

Tendon attaches to bone through a fibrocartilaginous transition zone (the 'enthesis' or 'insertion site') which functions to transfer load between two very different materials (Benjamin et al., 2002; Woo et al., 1987). Using the terminology of Benjamin et al., this load transfer can occur through a fibrocartilaginous enthesis (typically over a small area, e.g., the supraspinatus tendon of the rotator cuff) or through a fibrous enthesis (typically over long area, e.g., the medial collateral ligament) (Benjamin et al., 2002). It is expected that stress concentrations would arise at the interface of these two materials. The enthesis is prone to injury, and generally heals poorly (Fujioka et al., 1998; Leddy and Packer, 1977; Rodeo et al., 1993; St. Pierre et al., 1995; Thomopoulos et al., 2002, 2003a). Repair of the rotator cuff tendon to bone insertion, for example, is at high risk for early failure (Galatz et al., 2004; Harryman et al., 1991). The incidence of recurrence of injury after massive rotator cuff injury and repair has been reported to be as high as 94% (Galatz et al., 2004). Understanding the mechanical behavior of the *normal* tendon to bone insertion will allow for the development of devices and tissue engineering replacements to improve the repair.

*Corresponding author. Tel.: +1 314 362 8650; fax: +1 314 362 0334.
E-mail address: thomopouloss@msnotes.wustl.edu (S. Thomopoulos).

0021-9290/$ - see front matter © 2005 Elsevier Ltd. All rights reserved.
doi:10.1016/j.jbiomech.2005.05.021

The fibrocartilaginous tendon to bone insertion site has classically been categorized into four zones (Benjamin et al., 2002; Woo et al., 1987). It was previously demonstrated that the structure, composition, and the mechanical properties of the normal insertion varies along these zones (Fukuta et al., 1998; Niyibizi et al., 1996; Raspanti et al., 1996; Thomopoulos et al., 2003b; Waggett et al., 1998). The first zone consists of tendon proper, and is composed of well aligned type I collagen fibers with small amounts of the proteoglycan decorin. The second zone consists of fibrocartilage and is composed of types II and III collagen, with small amounts of types I, IX, and X collagen, and small amounts of the proteoglycans aggrecan and decorin. The third zone contains mineralized fibrocartilage and the predominant collagen is type II, with significant amounts of type X collagen as well as aggrecan. The border between these two fibrocartilaginous regions is demarcated by a "tidemark", a basophilic line that represents the calcification front. Finally, zone four consists of bone, which is made up predominantly of type I collagen with a high mineral content. It has been proposed that this continuous change in tissue composition and structure is necessary to minimize stress concentrations and aid in the efficient transfer of load between tendon and bone (Benjamin et al., 1992, 2002; Matyas et al., 1995; Thomopoulos et al., 2003b). However, the mechanism by which structure (i.e., collagen organization) and variation in mechanical properties minimizes stress concentrations has not been elucidated.

The objective of our study was to determine whether there is a *microstructural* basis for minimizing stress concentrations at the tendon to bone insertion site. We hypothesized that collagen fiber organization at the insertion is optimized to minimize the stress concentrations that would develop at the interface of the two materials (tendon and bone).

2. Methods

2.1. Experimental studies

Supraspinatus tendon to bone insertions from 5 male, 5–6 months old, skeletally mature, Fisher 344 rats were dissected free of surrounding tissues. Specimens were fixed in 10% buffered formalin with the tendon oriented parallel to the humerus (i.e., equivalent to a shoulder position of approximately 90° abduction). Applying tension to the tendon during fixation could affect collagen fiber orientation. Since an appropriate in vivo tension is unknown, the tendons in our study were fixed under zero tension. Specimens were processed for standard paraffin embedded histology and sectioned in the transverse plane (5 μm section thickness). All animal procedures were in compliance with the Animal Studies Committee regulations at Washington University School of Medicine. Sections were stained with 0.1% Picrosirius Red solution, destained in 1% acetic acid, counterstained with hematoxylin, and differentiated in 1% HCl in 70% ethanol. Collagen fiber angle distributions were measured at 5 locations along the length of the insertion, both in the fibrocartilage (FC) zone and in the mineralized fibrocartilage zone (MC), at positions on both sides of the tidemark (points A–E in Fig. 1), for a total of 10 locations per specimen. Sampling positions were chosen at 5 equidistant points along the arc defined by the supraspinatus tendon insertion tidemark. The endpoints (A and E in Fig. 1) were chosen based on the clearly evident edges of the tendon. When defining a sampling point in the mineralized vs. the un-mineralized portions of the insertion, 0.5 mm^2 areas were sampled on either side of the tidemark, ensuring that the area did not encroach over the tidemark line. A polarized light method for quantitative collagen orientation analysis was used to quantify collagen fiber orientation at each location (Dickey et al., 1998; Thomopoulos et al., 2003a, b; Whittaker and Canham, 1991). Tissue sections were documented and analyzed using a polarized light microscope (Olympus BX51P) and an Olympus DP70 digital microscope camera (36 bit, color, 1360 × 1040, 2/3 in CCD chip). The specimen was illuminated with light filtered through a crossed polarizer (east–west position) and analyzer (north–south position) (Bennett, 1964). Images were captured at section orientations from 45° to 135° in 5° increments (the long axis of the tendon was aligned with 90°). A compensator ($\lambda/4$ wave plate) was then engaged in a diagonal position (NW–SE) and additional images were recorded at section orientations from 45° to 135° in 5° increments. Software designed with Matlab (The Mathworks, Natick, MA) was used to determine the angle of extinction (θ). The software's graphical interface allows the user to interactively vary inputs such as the area of interest and the sampling frequency. An image of the tissue illuminated with linearly polarized light is displayed. A grid is overlaid on the image and defines the points of interest for analysis. A plot of light intensity vs. section orientation for each point of interest is then created. θ was determined by examining the plot of light intensity vs. section orientation and then locating the angle associated with the minimum light intensity. θ was determined at each point on the grid (note that each grid point consisted of a 3 × 3 pixel square). In order to determine whether the collagen orientation was at θ or $\theta \pm 90°$ (i.e., whether the slow axis of the collagen is aligned with the analyzer or the polarizer), the color hue was examined at $\theta \pm 45°$ using images taken with the compensator in place. A histogram was generated to display the distribution of collagen fiber orientations for all of the pixel bundles. The angular deviation of the collagen orientations for all pixel bundles was then calculated (Karlon et al., 1999).

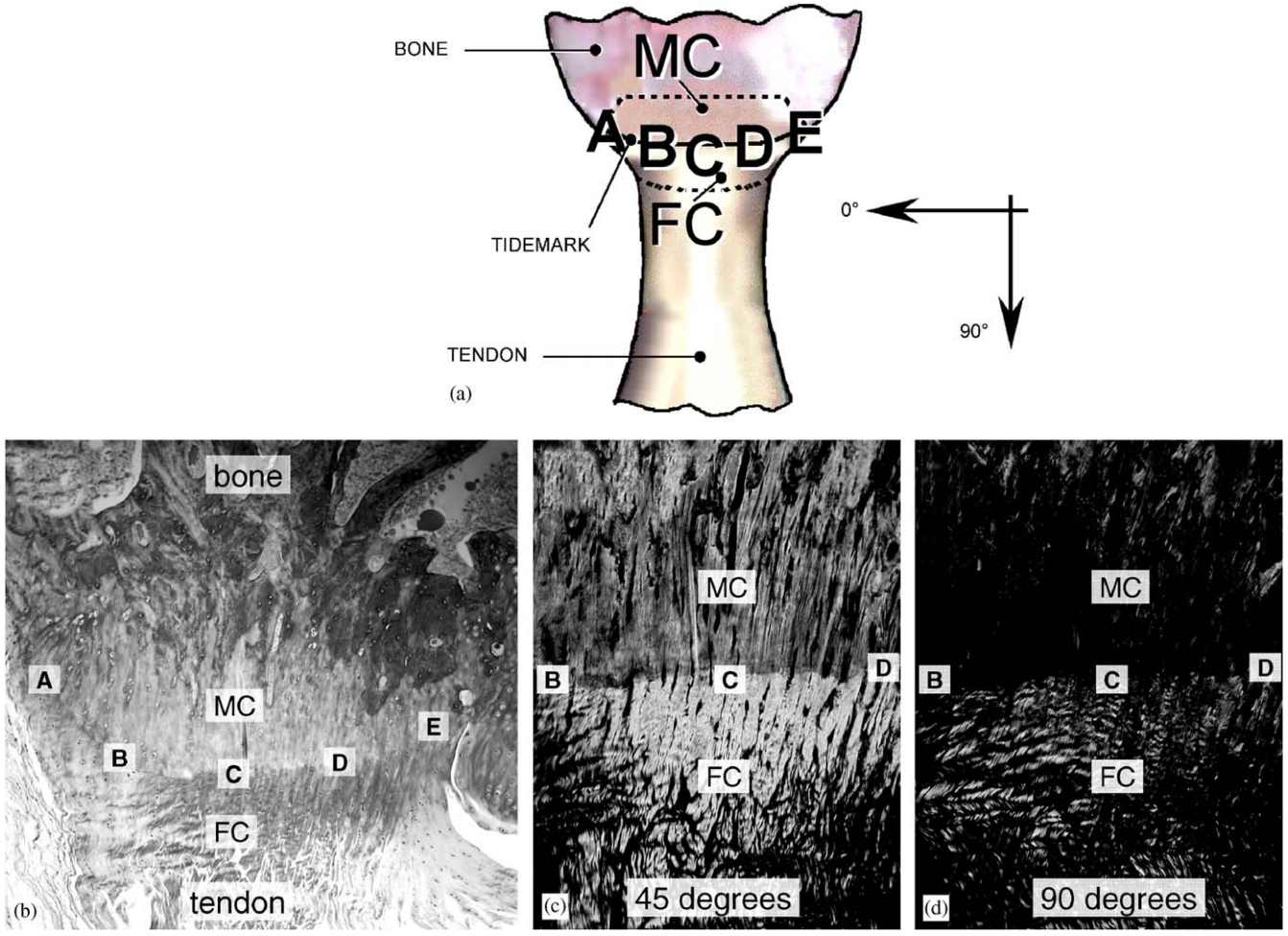

Fig. 1. (a) Collagen orientations were measured at 5 locations (A–E) on both sides of the tidemark (MC, FC). (b) A representative image of the insertion site under brightfield microscopy (Picrosirius Red stain, 10 × objective). (c) The specimen at a higher magnification (20 × objective) under polarized light microscopy. The tendon is oriented 45° relative to the orientation of the polarizer. (d) The tendon aligned with orientation of the polarizer. Note the decreased light intensity when the collagen fibers are aligned with the polarizer.

The tangent angle of the tidemark was also measured at the same five locations. The gross geometry of the insertion site was measured using direct optical imaging (a 200 mm macro lens, an Olympus DP70 digital camera, and Scion Image analysis software [Scion Corporation, Frederick, MD]).

Angular deviation was compared by location (A–D) and by tissue (FC, MC) using a two factor ANOVA followed by a Fischer's least squares differences post hoc test. Significance was set to $p < 0.05$.

2.2. Finite element studies

Plane stress finite element (FE) models were developed using ADINA (ADINA Research and Development, Watertown, MA) and Matlab. These models incorporated a highly simplified two-dimensional idealization of the insertion geometry, published variations in axial mechanical properties for tendon, bone, MC, and FC (Thomopoulos et al., 2003a, b), and stiffness matrices derived from measured collagen orientation distributions (Lanir, 1983; Zahalak et al., 2000).

The insertion was idealized macroscopically as in Fig. 2. The geometry was based on the observed geometry of rat supraspinatus insertions, but idealized to be symmetric about the midline. This symmetry was enforced by restraining points along the right-hand boundary of the model from displacing horizontally. The bone at the base of the MC region was modeled as rigid by restraining points along the bone–MC interface ("1" in Fig. 2) from displacing. The tidemark ("2" in Fig. 2) followed the measured shape (CDE in Fig. 1). The FC region ("2–3" in Fig. 2) followed measured dimensions. Beneath this, the tendon was assigned a uniform cross-section. Points along a line far from the

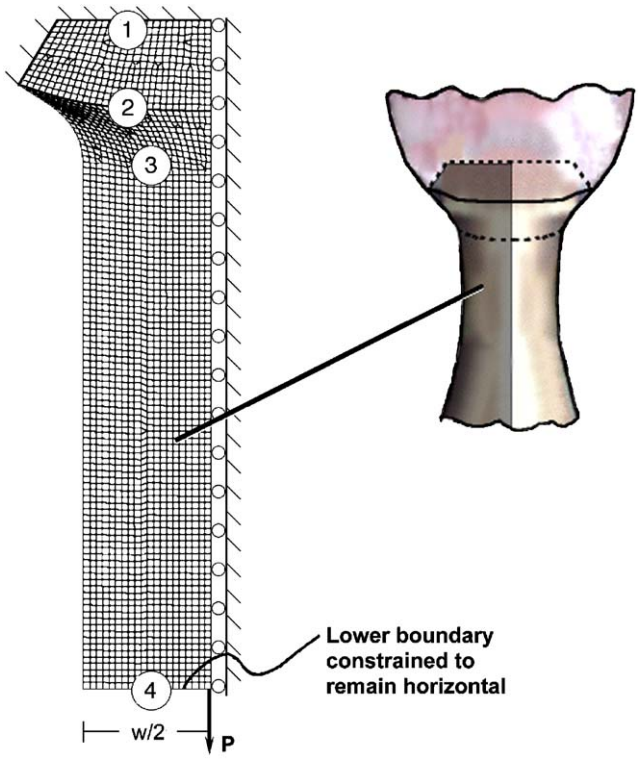

Fig. 2. The insertion was idealized macroscopically based on the observed geometry of rat supraspinatus tendon insertions. The bone at the base of the MC region was modeled as rigid by restraining points along the bone–MC interface (1) from displacing. The tidemark (2) followed the measured shape. The FC region (2–3) followed measured dimensions. Points along a line far from the interface (4) were displaced uniformly and stress was monitored.

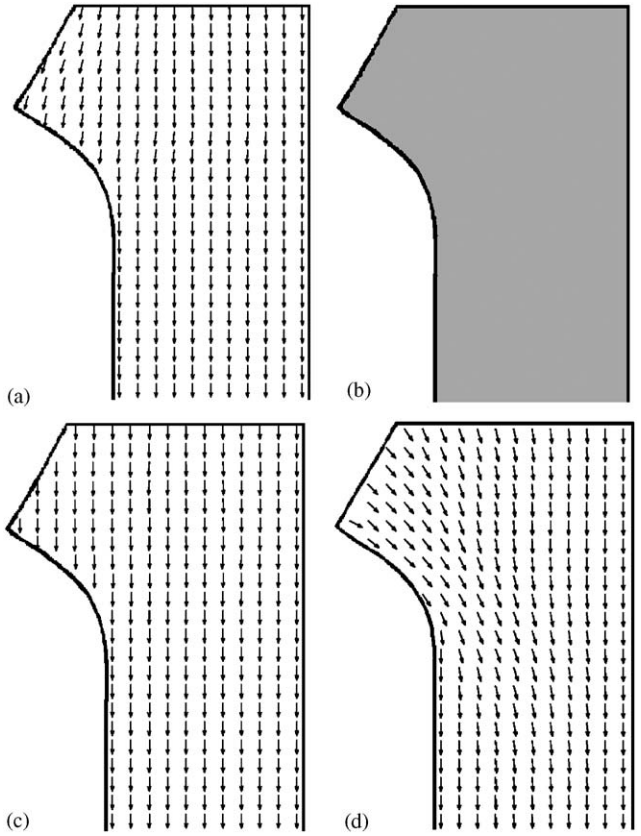

Fig. 3. Distribution of mean collagen fiber orientation angle for the (a) physiologic case, (b) random (i.e., isotropic) case, (c) orthotropic case, and (d) "optimized" case.

interface ("4" in Fig. 2) were displaced uniformly and the force P was monitored.

Models were assigned measured insertion thicknesses along curves 2 and 3 in Fig. 2, and linearly interpolated thicknesses t at all intermediate points. The thickness of curve 2 was $t/w = 0.25$; the thickness of curve 3 was $t/w = 0.125$. The thickness of the insertion below and above the FC region ("1–2" and "3–4" in Fig. 2) were assigned to be uniform. While these thickness to width ratios preclude the use of a plane stress model as a means of predicting stress fields in real insertion sites, the plane stress model was chosen as an idealized system in which to qualitatively assess how the measured planar variations in collagen fiber orientation affects stress transfer.

2.3. Tendon mechanical properties

Mechanical properties were derived from experimental measurements reported elsewhere (Thomopoulos et al., 2003a, b) and the measured collagen fiber orientation distribution. In addition to the physiologic collagen orientation case, three comparison cases were studied. The spatial distribution of the mean collagen fiber orientation angle for each case is depicted with arrows in Fig. 3. The cases modeled were: (a) the "physiologic" case (Fig. 3a), incorporating the experimentally determined distribution; (b) the "random" case (Fig. 3b), incorporating an isotropic distribution (with an undefined mean orientation angle), with Poisson's ratio $v = 0.5$; (c) the "orthotropic" case (Fig. 3c), incorporating a spatially uniform distribution of the fiber distribution mean angle, and the local angular deviation measured at point C (Fig. 1); and (d) an "optimized" distribution (Fig. 3d), with the local angular deviation identical to that measured at point C (Fig. 1), except that the mean fiber direction throughout the tendon and insertion was prescribed to follow the principal directions of stress and strain from the isotropic case. In each case, the local stiffness matrix and spatial distribution of mechanical properties were determined as follows.

2.4. Stiffness matrix at each point

Individual collagen fibers were idealized as linear elastic and orthotropic, with isotropy in their cross-sectional plane (the b–c plane in Fig. 4). Overall tendon material properties were found by summing the in-

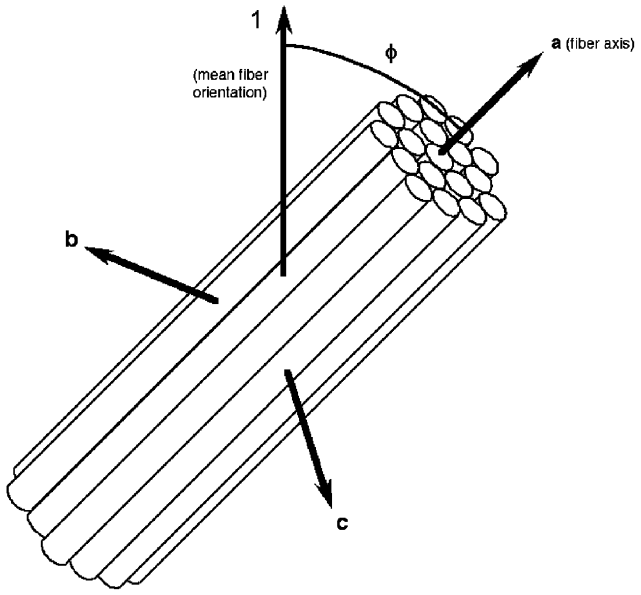

Fig. 4. Collagen fiber axes (*a,b,c*), oriented a "nutation" angle of ϕ from the mean orientation of collagen fibers at a point (the 1-direction).

dividual contributions of the fibers according to a spherically symmetric generalization of the observed orientation distribution.

Fibers were assigned an axial modulus, E_a, chosen so that the overall tendon properties matched experimentally measured values. The remaining properties were chosen to be representative of a loosely bound bundle of fibrils. The stiffnesses E_b and E_c (Fig. 4) in the transverse directions were set at a small fraction of the E_a ($E_b = E_c = 0.015E_a$), based upon the observations of Lynch et al. (2003) and Weiss et al. (2002). The Poisson's ratios for axial contraction (*a*-direction), contraction caused by lateral (*bc*-plane) straining, were set close to zero ($\nu_{ba} = \nu_{ca} = 0.0075$). With these prescribed, the thermodynamic requirement that $\nu_{ab}/E_a = \nu_{ba}/E_b$ (Jones, 1999) then dictated that $\nu_{ab} = \nu_{ac} = 0.5$. ν_{bc} and ν_{cb} were set to 0.9925, which is as close to 1 as allowed by the following constraint (Jones, 1999):

$$1 - \nu_{bc}\nu_{cb} - \nu_{ba}\nu_{ab} - \nu_{ca}\nu_{ac} - \nu_{ba}\nu_{cb}\nu_{ac} > 0. \tag{1}$$

These are appropriate for diagonal packing of fibers; the high Poisson's ratios for compressing a bundle of fibers is a consequence of the rigid body kinematics (e.g., Ginsberg and Genin, 1995) of sliding fibers. The shear moduli G_{ab} and G_{bc} were set at 0.001 E_a, and G_{ac} was set at 0.005 E_a. The low relative values of shear moduli are appropriate for aligned bundles of slender fibers (e.g., Evans and Zok, 1994). These values were considered reasonable since, when combined, they reproduced experimental observations of tendon properties. These values enter into the stiffness tensor for each fiber, $\mathbf{C}^{(f)}$, in the usual way (Jones, 1999), yielding a relation between the stress $\boldsymbol{\sigma}^{(f)}$ and strain $\boldsymbol{\varepsilon}^{(f)}$ in each fiber:

$$\boldsymbol{\sigma}^{(f)} = \mathbf{C}^{(f)}\boldsymbol{\varepsilon}^{(f)}. \tag{2}$$

The total stress $\boldsymbol{\sigma}$ at a point in the tendon is the sum of the stresses in all fibers crossing that point (boldface indicates tensors of rank greater than zero.) The stress in a region Ω of a tendon in which the volume fraction of fibers is f is then

$$\boldsymbol{\sigma} = \int_\Omega f\boldsymbol{\sigma}^{(f)}(\mathbf{n})p(\mathbf{n})\,d\Omega = \int_\Omega f\mathbf{C}^{(f)}\boldsymbol{\varepsilon}^{(f)}(\mathbf{n})p(\mathbf{n})\,d\Omega, \tag{3}$$

where $p(\mathbf{n})$ is the probability of finding a fiber whose axis is parallel to the unit vector $\mathbf{n}$, and $\boldsymbol{\sigma}^{(f)}(\mathbf{n})$ and $\boldsymbol{\varepsilon}^{(f)}(\mathbf{n})$ are the stress and strain tensors in such a fiber. Note that the integral of $p(\mathbf{n})$ over the region Ω must equal one. Applying the continuum assumption that the local strain field $\boldsymbol{\varepsilon}^{(f)}$ in each fiber equals the macroscopic tissue strain $\boldsymbol{\varepsilon}$ at a point, Eq. (3) can be rewritten as

$$\boldsymbol{\sigma} = \left(\int_\Omega f\mathbf{C}^{(f)}p(\mathbf{n})\,d\Omega\right)\boldsymbol{\varepsilon} \equiv \mathbf{C}^{(t)}\boldsymbol{\varepsilon}, \tag{4}$$

where the term in parentheses defines the local tendon stiffness tensor $\mathbf{C}^{(t)}$.

Several generalizations of normal probability distributions to cylindrical and spherical coordinates exist (Fisher et al., 1987; Leong and Carlile, 1998). The distribution function we adopted is spherically symmetric, such that the "nutation" angle ϕ relative to the mean fiber direction at a point (Fig. 4) is the only directional variable. For such a case, the following is a reasonable generalization of the normal distribution for $-\pi/2 \leqslant \phi \leqslant \pi/2$:

$$p(\phi) = \frac{e^{-(\phi^2)/2s^2}}{\sqrt{2\pi}se^{-(s^2)/2}}, \tag{5}$$

where s is the measured angular deviation of the fiber distribution in radians.

The final step in determining the stiffness matrix at a point was determining the appropriate magnitude of the fiber axial stiffness E_a at each point. This was found by calibrating the longitudinal elastic modulus of the tendon, $E^{(t)}_{long}$, to measured values.

$$E_a = \frac{E^{(t)}_{long}}{\bar{E}}, \tag{6}$$

where, if the 1-direction lies parallel to the mean fiber direction at a point, $1/\bar{E}$ is the 1111 component of the inverse of $\mathbf{C}^{(t)}$.

2.5. Spatial distribution of mechanical properties

The mean direction and angular deviation of the fiber orientation distributions were interpolated from measured values along each side of the tidemark. In the MC, these values were assigned to vary in the 0°-direction, but not in the 90°-direction (Fig. 1). Orientation distributions were interpolated smoothly throughout the FC in both directions, from the tidemark to the tendon (line "3" in Fig. 2).

Measured axial stiffnesses (Thomopoulos et al., 2003a, b) corresponding to axial straining of 2% of material from the centerline of the insertion were used to calibrate E_a (cf. Eq. (5) in the MC, FC, and tendon. E_a was uniform in the MC, jumped at the tidemark, and was interpolated smoothly through the FC to the tendon.

3. Results

3.1. Experimental studies

The tidemark tangent angle varied from $-20°$ to $+15°$ (Fig. 5). The average collagen fiber angle varied from 83° to 98° at the FC and 86° to 103° at the MC. Collagen fibers did not always lie perpendicular to the tidemark. Fibers were significantly less organized at the edges of the insertion (locations A and E) compared to the middle of the insertion (location C). Fibers in the center were significantly more organized at the MC compared to the FC (Fig. 6).

3.2. Influence of statistical parameters on local mechanical properties

The spatial variation in angular deviation had a relatively small effect on local mechanical properties. The angular deviation varied from $s = 5°$ to 10° over the insertion. The difference between the engineering constants at points having these extreme values can be seen in Table 1, which shows that the case of $s = 10°$ is not appreciably closer to isotropy than the case of $s = 5°$.

This is also evident in the in-plane stiffness matrices. For the isotropic case, the in-plane matrix, normalized by E_a, is

$$\begin{bmatrix} \frac{1}{E_1} & \frac{-v_{21}}{E_2} & 0 \\ \frac{-v_{12}}{E_1} & \frac{1}{E_2} & 0 \\ 0 & 0 & \frac{1}{G_{12}} \end{bmatrix} = \begin{bmatrix} 1 & -0.5 & 0 \\ -0.5 & 1 & 0 \\ 0 & 0 & 0.333 \end{bmatrix}. \quad (7)$$

Here, E_1 is the elastic modulus for straining in the 1-direction, which is aligned with mean direction of the fiber orientation distribution at a point; E_2 is the elastic modulus for straining in the 2-direction, which is perpendicular to 1-direction; $-v_{12}$ is the ratio between the degree of the expansion in the 1-direction and

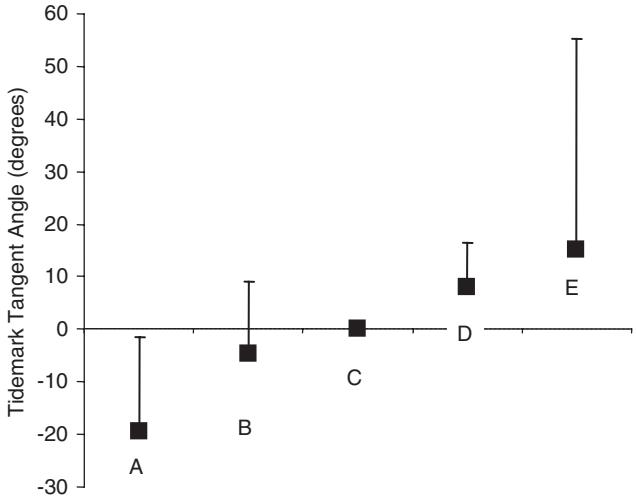

Fig. 5. The tidemark angle was measured at 5 locations (A–E in Fig. 1). The tidemark angle at location C was defined as 0°. The tangent angle varied considerably from location A to location E, demonstrating the curvature of the supraspinatus tendon insertion site.

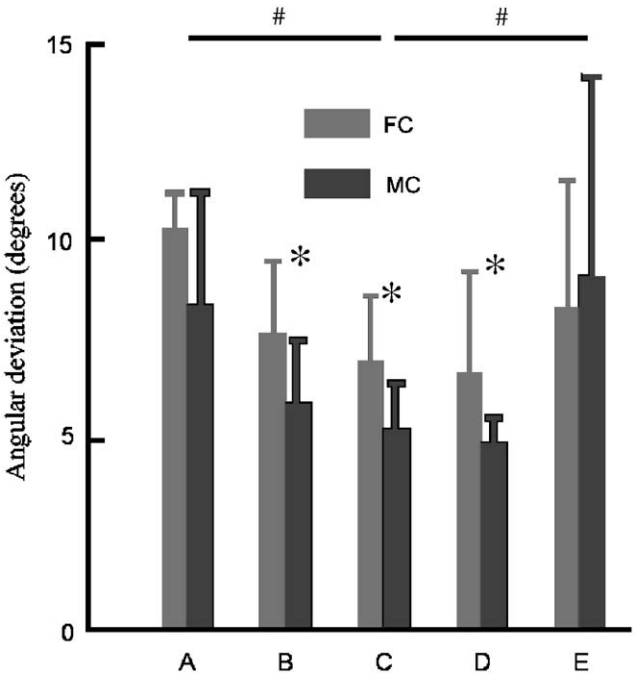

Fig. 6. Collagen orientations were measured at 5 locations (A–E) on both sides of the tidemark (MC, FC). The average collagen fiber angle varied from 83° to 98° at the FC and 86° to 103° at the MC. Collagen fibers did not always lie perpendicular to the tidemark. Fibers were significantly less organized at the edges of the insertion (locations A and E) compared to the middle of the insertion (location C) (# $p<0.05$). Fibers in the center were significantly more organized at the MC compared to the FC (* $p<0.05$).

Table 1
Variation in normalized engineering constants as a function of angular deviation, s

Isotropic	$s = 5^\circ$	$s = 10^\circ$
$E_1 = 1$	$E_1 = 1$	$E_1 = 1$
$E_2 = 1$	$E_2 = 0.0157$	$E_2 = 0.023$
$E_3 = 1$	$E_3 = 0.0157$	$E_3 = 0.023$
$v_{12} = 0.5$	$v_{12} = 0.0003$	$v_{12} = 0.0012$
$v_{13} = 0.5$	$v_{13} = 0.0003$	$v_{13} = 0.0012$
$v_{23} = 0.5$	$v_{23} = 0.992$	$v_{23} = 0.988$
$G_{12} = 0.333$	$G_{12} = 0.0154$	$G_{12} = 0.0565$
$G_{13} = 0.333$	$G_{13} = 0.0154$	$G_{13} = 0.0565$
$G_{23} = 0.333$	$G_{23} = 0.0039$	$G_{23} = 0.0058$

Increasing the angular deviation from $s = 5^\circ$ to 10° (the range of experimentally measured deviations) did not make the constants appreciably closer to the isotropic case.

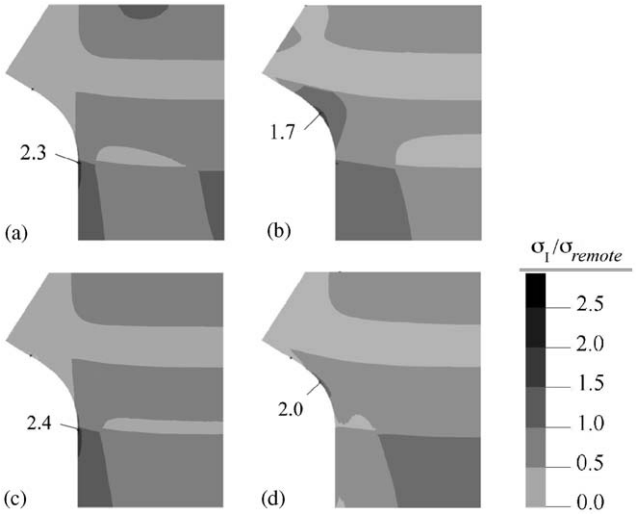

Fig. 7. Maximum principal stress, normalized by the average remote axial stress in the tendon for four cases of collagen organization, (a)–(d). In all cases, a stress concentration is evident near the insertion. In the physiologic and orthotropic cases, the stress concentration lies beneath the outward splay of the tendon, at the threshold of the FC region. In the random and "optimized" cases, the maximum was on the outward splay itself.

contraction in the 2-direction for uniaxial stressing in the 1-direction; $-v_{21}$ is the ratio between the degree of the expansion in the 2-direction and contraction in the 1-direction for uniaxial stressing in the 2-direction; and G_{12} is the shear modulus for shearing in the 1–2 plane (Jones, 1999). For the case of $s = 5^\circ$,

$$\begin{bmatrix} \frac{1}{E_1} & \frac{-v_{21}}{E_2} & 0 \\ \frac{-v_{12}}{E_1} & \frac{1}{E_2} & 0 \\ 0 & 0 & \frac{1}{G_{12}} \end{bmatrix} = \begin{bmatrix} 1 & -0.0191 & 0 \\ -0.0191 & 63.7 & 0 \\ 0 & 0 & 64.9 \end{bmatrix}. \quad (8)$$

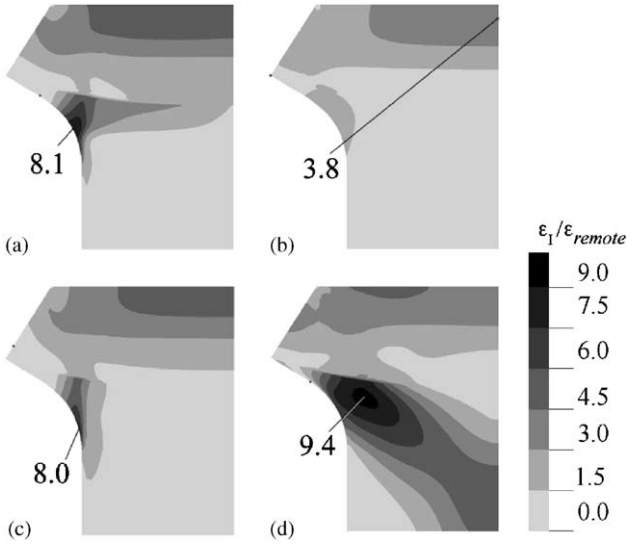

Fig. 8. Contours of maximum principal strain in each of the four cases considered. Strains were normalized by the remote maximum principal strain. Peak strains were highest in the "optimized" case, followed by the physiologic, orthotropic and, random (i.e., isotropic) cases.

For the case of $s = 10^\circ$,

$$\begin{bmatrix} \frac{1}{E_1} & \frac{-v_{21}}{E_2} & 0 \\ \frac{-v_{12}}{E_1} & \frac{1}{E_2} & 0 \\ 0 & 0 & \frac{1}{G_{12}} \end{bmatrix} = \begin{bmatrix} 1 & -0.0522 & 0 \\ -0.0522 & 43.5 & 0 \\ 0 & 0 & 17.7 \end{bmatrix}. \quad (9)$$

3.3. FE studies

Stress and strain fields were calculated for the four cases described above. Maximum principal stress is shown in Fig. 7, normalized by the average remote axial stress in the tendon. In all cases, a stress concentration is evident near the insertion. In the physiologic and orthotropic cases, the stress concentration lies beneath the outward splay of the tendon, at the threshold of the FC region. In the random and "optimized" cases, the maximum was on the outward splay itself. The stress concentrations (maximum principal Cauchy stress normalized by the applied stress) were: (1) physiologic case: 2.3, (2) random (i.e., isotropic) case: 1.7, (3) orthotropic case: 2.4, and (4) "optimized" case: 2.0.

As shown in Fig. 8, peak strains were highest in the "optimized" case, followed by the physiologic, orthotropic and random (i.e., isotropic) cases.

4. Discussion

The tendon to bone insertion transfers loads from a relatively compliant tendon to a relatively stiff bone. The obstacle that must be overcome through its macroscopic shape and average collagen orientation is that stress singularities can exist at the interface between two dissimilar materials. If the combination of macroscopic and microscopic morphology allows stresses to be transmitted to a sharp corner, stresses can be enormous at this corner (Genin and Hutchinson, 1997; Williams, 1952).

In this work, we measured the average collagen orientation along the insertion, and examined how this architecture affects load transfer in an idealized tendon to bone insertion. The angular deviation of the collagen microstructure dictates the directional variation in stiffness of the insertion at each point. Using a spherical probability distribution and treating collagen fibers as nearly uniaxial elements, we found that mechanical orthotropy (ratio of maximum to minimum tensile stiffness at a point) varied by about 50% over the entire insertion. However, this variation was not mechanically significant, as it represented a variation from 1.6% to 2.3% of the value needed for isotropy (Table 1).

The spatial variation of the mean orientation angle of the collagen fiber distribution had a strong effect on the way that the insertion transfers mechanical stresses. This was studied through a series of finite element analyses of idealized insertions. The stress concentration was lowest for the case of a random (isotropic) distribution of collagen fibers, but this came at the cost of having a stress concentration on the outward splay of the insertion, and at the cost having collagen fibers that bear no load. For the tissue studied, about 2.6 times the volume of collagen would be needed to create an isotropic tissue with the same axial stiffness as the tendon insertions studied (Fig. 9). The other extreme case, that of an orthotropic insertion whose mean orientation angle paralleled the tendon axis, had a high stiffness to volume ratio and moved the peak stress concentration to the tendon, but the low shear modulus of tissue in the splay led to the highest stress concentration of the four cases studied. The "optimized" morphology that one familiar with Wolff's Law in bone might expect did indeed reduce the stress concentration, but this resulted in a peak stress on the outward splay of the tendon (Fig. 7), a peak strain within the FC (Fig. 8), and a slightly more compliant insertion (Fig. 9).

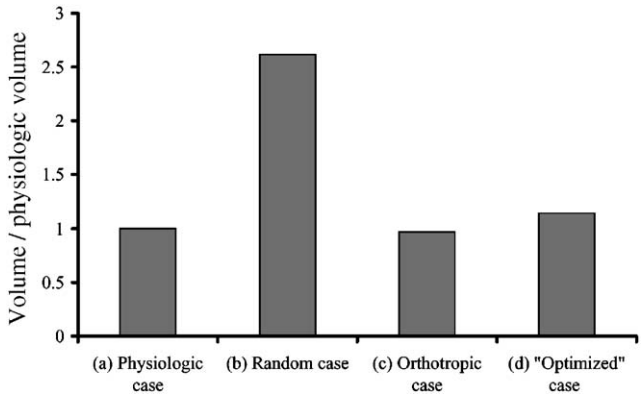

Fig. 9. Thickness scaling needed to achieve the physiologic tendon-insertion stiffness. About 2.6 times the volume of collagen would be needed to create an isotropic tissue with the same axial stiffness as the tendon insertions studied.

Natural tendon to bone insertions are a balanced trade-off between the best features of the other three models examined. Fibers are nearly aligned to improve the stiffness to volume ratio. However, fibers run nearly perpendicular to the tidemark at the tendon to bone insertion. This reduces the stiffness in the direction of the highest stress gradient, which reduces overall stresses. On the outward splay, fibers deviate towards the normal of the splay. The resulting reduction in stiffness along the boundary of the splay increases the strain concentration, but reduces the stress concentration.

Other groups have also modeled the mechanical behavior of tendons, ligaments, and their insertions using different approaches. Puso et al. developed an anisotropic, viscoelastic, three-dimensional model of the medial collateral ligament (Puso and Weiss, 1998). The model accurately reproduced the anisotropy and the time-dependent behavior of dense connective tissues. The model, however, did not accurately describe the ligament–bone insertion because the site was represented as a sudden transition from ligament material to bone material. The anterior cruciate ligament was modeled in a different study by Song et al. (Song et al., 2004). The mechanical behavior of the tissue was modeled using an exponential strain energy function, and the finite element results were validated with experimental mechanical test data. This three-dimensional model effectively described the interaction of the ligament bundles and the surrounding structures of the knee. The study, however, was not designed to study the ligament–bone insertions. The ligament–bone insertion was again modeled as a sudden transition from ligament material to bone material.

Two other studies focused on the effect of the stress environment on cells in compressive regions of tendon or ligament (Giori et al., 1993; Matyas et al., 1995). Matyas et al. found that cell shape correlated with principal and hydrostatic stresses at the medial collateral ligament insertion site predicted using a two-dimensional, linearly elastic, isotropic finite element model. This first order approximation demonstrated that stress environment influences the behavior of cells. Giori et al.

similarly showed using a two-dimensional finite element analysis that cartilaginous tissue regions correlated well with a compressive stress environment, while fibrous matrix regions correlated well with tensile stresses. Their tissue was modeled as a homogenized two phase fiber-reinforced composite. Our results are consistent with these two studies. While we looked at the effect of collagen fiber orientation on the stresses at the insertion site, and not at the effect of the stress environment on cell behavior, we also found a variation in properties along the insertion site. Collagen orientation varied along the insertion, with consequences on the predicted stress concentrations. These stress concentrations may influence the cell shape and the matrix production, as described by Giori et al. (1993) and by Matyas et al. (1995).

The results presented in this paper must be interpreted only in the context of the underlying idealizations. The limitations of approximating tissue behavior with linearized kinematics and linear constitutive behavior are very well established (Prager, 1969), and the conclusions drawn in this paper must be recognized as first-order estimates. The idealized geometry might miss important mechanisms for stress transfer out of plane, and we emphasize that the numerical results show only the qualitative effect of the measured fiber orientation distributions on stress transfer. Milz et al. demonstrated that there is a complex three-dimensional pattern of interlocking surfaces between mineralized fibrocartilage and bone (Milz et al., 2002), which must be accounted for to understand how fiber orientation distributions in the out-of-plane direction affect stress transfer. The idealized constitutive representation accounts for spatial variations of material properties, but focuses on the role of collagen orientation, which is the major factor in tendon mechanics. Elastic nonlinearity (Genin and Hutchinson, 1997) and viscoelastic damping (Cairns et al., 1999) may amplify or reduce stress concentrations. Future work must account for how three-dimensional morphology, three-dimensional fiber architecture, and geometric and material non-linearity affect stress transfer.

The tendon to bone insertion in the rat supraspinatus tendon appears to be optimized to reduce stress concentrations and shield the outward splay of the tendon. The local fiber architecture was found to deviate only slightly from the tendon axis in its mean orientation, and the local angular deviation ($5^\circ < s < 10^\circ$) was fairly uniform across the insertion. However, local variations in mean fiber angle were shown to have a very strong effect on the way load is transferred from tendon to bone. This motivates future attempts to improve surgical reattachment procedures by augmenting tendon stiffness with functionally graded tissue constructs, or by guiding collagen to remodel into optimal fiber architectures.

Acknowledgment

Funding- NIH 5R01AR047591-04.

References

Benjamin, M., Newell, R.L., Evans, E.J., Ralphs, J.R., Pemberton, D.J., 1992. The structure of the insertions of the tendons of biceps brachii, triceps and brachialis in elderly dissecting room cadavers. Journal of Anatomy 180, 327–332.

Benjamin, M., Kumai, T., Milz, S., Boszczyk, B.M., Boszczyk, A.A., Ralphs, J.R., 2002. The skeletal attachment of tendons—tendon "entheses". Comparative Biochemistry and Physiology. A Molecular and Integrative Physiology 133, 931–945.

Bennett, S.H., 1964. Methods applicable to the study of both fresh and fixed materials. In: Jones, R.M. (Ed.), McClung's Handbook of Microscopic Technique. Hafner Publishing Co., New York, pp. 591–677.

Cairns, D.R., Genin, G.M., Wagoner, A., Crawford, G., 1999. Amplified strain-rate dependence of deformation in polymer dispersed liquid crystal materials. Applied Physics Letters 75, 1872–1874.

Dickey, J.P., Hewlett, B.R., Dumas, G.A., Bednar, D.A., 1998. Measuring collagen fiber orientation: a two-dimensional quantitative macroscopic technique. Journal of Biomechanical Engineering 120, 537–540.

Evans, A.G., Zok, F.W., 1994. The physics and mechanics of fiber-reinforced brittle matrix composites (review). Journal of Material Science 29, 3857–3896.

Fisher, N.I., Lewis, T., Embleton, B.J.J., 1987. Statistical Analysis of Spherical Data. Cambridge University Press, New York.

Fujioka, H., Thakur, R., Wang, G.J., Mizuno, K., Balian, G., Hurwitz, S.R., 1998. Comparison of surgically attached and non-attached repair of the rat Achilles tendon-bone interface. Cellular organization and type X collagen expression. Connective Tissue Research 37, 205–218.

Fukuta, S., Oyama, M., Kavalkovich, K., Fu, F.H., Niyibizi, C., 1998. Identification of types II, IX and X collagens at the insertion site of the bovine achilles tendon. Matrix Biology 17, 65–73.

Galatz, L.M., Ball, C.M., Teefey, S.A., Middleton, W.D., Yamaguchi, K., 2004. The outcome and repair integrity of completely arthroscopically repaired large and massive rotator cuff tears. Journal of Bone and Joint Surgery—American Volume 86-A, 219–224.

Genin, G.M., Hutchinson, J.W., 1997. Composite laminates in plane stress: constitutive modeling, and stress redistribution due to matrix cracking. Journal of the American Ceramic Society 80, 1245–1255.

Ginsberg, J.H., Genin, J., 1995. Dynamics, second ed. PWS Publishing Co., New York.

Giori, N.J., Beaupre, G.S., Carter, D.R., 1993. Cellular shape and pressure may mediate mechanical control of tissue composition in tendons. Journal of Orthopaedic Research 11, 581–591.

Harryman II, D.T., Mack, L.A., Wang, K.Y., Jackins, S.E., Richardson, M.L., Matsen III, F.A., 1991. Repairs of the rotator cuff. Correlation of functional results with integrity of the cuff. Journal of Bone and Joint Surgery 73, 982–989.

Jones, R.M., 1999. Mechanics of Composite Materials, second ed. Taylor & Francis, Inc., Philadelphia.

Karlon, W.J., Hsu, P.P., Li, S., Chien, S., McCulloch, A.D., Omens, J.H., 1999. Measurement of orientation and distribution of cellular alignment and cytoskeletal organization. Annals of Biomedical Engineering 27, 712–720.

Lanir, Y., 1983. Constitutive equations for fibrous connective tissues. Journal of Biomechanics 16, 1–12.

Leddy, J.P., Packer, J.W., 1977. Avulsion of the profundus tendon insertion in athletes. Journal of Hand Surgery—American Volume 2, 66–69.

Leong, P., Carlile, S., 1998. Methods for spherical data analysis and visualization. Journal of Neuroscience Methods 80, 191–200.

Lynch, H.A., Johannessen, W., Wu, J.P., Jawa, A., Elliott, D.M., 2003. Effect of fiber orientation and strain rate on the nonlinear uniaxial tensile material properties of tendon. Journal of Biomechanical Engineering 125, 726–731.

Matyas, J.R., Anton, M.G., Shrive, N.G., Frank, C.B., 1995. Stress governs tissue phenotype at the femoral insertion of the rabbit MCL. Journal of Biomechanics 28, 147–157 [see comments].

Milz, S., Rufai, A., Buettner, A., Putz, R., Ralphs, J.R., Benjamin, M., 2002. Three-dimensional reconstructions of the Achilles tendon insertion in man. Journal of Anatomy 200, 145–152.

Niyibizi, C., Sagarrigo Visconti, C., Gibson, G., Kavalkovich, K., 1996. Identification and immunolocalization of type X collagen at the ligament-bone interface. Biochemical and Biophysical Research Communications 222, 584–589.

Prager, W., 1969. On the formulation of constitutive equations for living soft tissues. Applied Mathematics 27, 128–132.

Puso, M.A., Weiss, J.A., 1998. Finite element implementation of anisotropic quasi-linear viscoelasticity using a discrete spectrum approximation. Journal of Biomechanical Engineering 120, 62–70.

Raspanti, M., Strocchi, R., De Pasquale, V., Martini, D., Montanari, C., Ruggeri, A., 1996. Structure and ultrastructure of the bone/ligament junction. Italian Journal of Anatomy and Embryology 101, 97–105.

Rodeo, S.A., Arnoczky, S.P., Torzilli, P.A., Hidaka, C., Warren, R.F., 1993. Tendon-healing in a bone tunnel. A biomechanical and histological study in the dog. Journal of Bone and Joint Surgery—American Volume 75, 1795–1803.

Song, Y., Debski, R.E., Musahl, V., Thomas, M., Woo, S.L., 2004. A three-dimensional finite element model of the human anterior cruciate ligament: a computational analysis with experimental validation. Journal of Biomechanics 37, 383–390.

St. Pierre, P., Olson, E.J., Elliott, J.J., O'Hair, K.C., McKinney, L.A., Ryan, J., 1995. Tendon-healing to cortical bone compared with healing to a cancellous trough. A biomechanical and histological evaluation in goats. Journal of Bone and Joint Surgery—American Volume 77, 1858–1866.

Thomopoulos, S., Hattersley, G., Rosen, V., Mertens, M., Galatz, L., Williams, G.R., Soslowsky, L.J., 2002. The localized expression of extracellular matrix components in healing tendon insertion sites: an in situ hybridization study. Journal of Orthopaedic Research 20, 454–463.

Thomopoulos, S., Williams, G.R., Soslowsky, L.J., 2003a. Tendon to bone healing: differences in biomechanical, structural, and compositional properties due to a range of activity levels. Journal of Biomechanical Engineering 125, 106–113.

Thomopoulos, S., Williams, G.R., Gimbel, J.A., Favata, M., Soslowsky, L.J., 2003b. Variation of biomechanical, structural, and compositional properties along the tendon to bone insertion site. Journal of Orthopaedic Research 21, 413–419.

Waggett, A.D., Ralphs, J.R., Kwan, A.P., Woodnutt, D., Benjamin, M., 1998. Characterization of collagens and proteoglycans at the insertion of the human Achilles tendon. Matrix Biology 16, 457–470.

Weiss, J.A., Gardiner, J.C., Bonifasi-Lista, C., 2002. Ligament material behavior is nonlinear, viscoelastic and rate-independent under shear loading. Journal of Biomechanics 35, 943–950.

Whittaker, P., Canham, P.B., 1991. Demonstration of quantitative fabric analysis of tendon collagen using two-dimensional polarized light microscopy. Matrix 11, 56–62.

Williams, M.L., 1952. Stress singularities resulting from various boundary conditions in angular corners of plates in extension. Journal of Applied Mechanics 19, 526–528.

Woo, S.L., Maynard, J., Butler, D., 1987. Ligament, tendon, and joint capsule insertions to bone. In: Woo, S.L. (Ed.), Injury and Repair of the Musculoskeletal Soft Tissues. American Academy of Orthopaedic Surgeons, Savannah GA, pp. 129–166.

Zahalak, G.I., Wagenseil, J.E., Wakatsuki, T., Elson, E.L., 2000. A cell-based constitutive relation for bio-artificial tissues. Biophysical Journal 79, 2369–2381.